INVESTIGATION OF THE SUCTION SYSTEM AND BOUNDARY-LAYER CHARACTERISTICS ON A HIGH-LIFT, BLC L-19 TEST AIRCRAFT

L. J. Mertaugh, et al

Mississippi State University

Prepared for:

Army Air Mobility Research and Development Laboratory

May 1973

AD

USAAMRDL TECHNICAL REPORT 73-2

INVESTIGATION OF THE SUCTION SYSTEM AND BOUNDARY-LAYER CHARACTERISTICS ON A HIGH-LIFT, BLC L-19 TEST AIRCRAFT

By

L. J. Mertaugh

S. Burt

May 1973

EUSTIS DIRECTORATE

U. S. ARMY AIR MOBILITY RESEARCH AND DEVELOPMENT LABORATORY

FORT EUSTIS, VIRGINIA

CONTRACT DAAJ02-67-C-0016

DEPARTMENT OF AEROPHYSICS AND AEROSPACE ENGINEERING

MISSISSIPPI STATE UNIVERSITY

STATE COLLEGE, MISSISSIPPI

37

DISCLAIMERS

The findings in this report are not to be construed as an official Department of the Army position unless so designated by other authorized documents.

When Government drawings, specifications, or other data are used for any purpose other than in connection with a definitely related Government procurement operation, the U.S. Government thereby incurs no responsibility nor any obligation whatsoever; and the fact that the Government may have formulated, furnished, or in any way supplied the said drawings, specifications, or other data is not to be regarded by implication or otherwise as in any manner licensing the holder or any other person or corporation, or conveying any rights or permission, to manufacture, use, or sell any patented invention that may in any way be related thereto.

Trade names cited in this report do not constitute an official endorsement or approval of the use of such commercial hardware or software.

DISPOSITION INSTRUCTIONS

Destroy this report when no longer needed. Do not return it to the originator.

DEPARTMENT OF THE ARMY
U S ARMY AIR MOBILITY RESEARCH & DEVELOPMENT LABORATORY
EUSTIS DIRECTORATE
FORT EUSTIS, VIRGINIA 23604

This report has been reviewed by the U. S. Army Air Mobility Research and Development Laboratory, and is considered to be technically sound. The report is published for the exchange of information and the stimulation of ideas. The program was conducted under the technical management of Mr. Frederick A. Raitch of the Technology Applications Division of this Directorate.

Task 1F162204A14234
Contract DAAJ02-67-C-0016
USAAMRDL Technical Report 73-2
May 1973

INVESTIGATION OF THE SUCTION SYSTEM AND BOUNDARY-LAYER CHARACTERISTICS ON A HIGH-LIFT, BLC L-19 TEST AIRCRAFT

AASE Report No. 72-70

By

L. J. Mertaugh
S. Burt

Prepared by

Department of Aerophysics and Aerospace Engineering
Mississippi State University
State College, Mississippi

for

EUSTIS DIRECTORATE
U. S. ARMY AIR MOBILITY RESEARCH AND DEVELOPMENT LABORATORY
FORT EUSTIS, VIRGINIA

ABSTRACT

This report presents the results of a test program which was intended to document the boundary-layer control system characteristics of the high-lift L-19 aircraft. This aircraft incorporates a distributed-suction, turbulent-boundary-layer control system which allows trimmed lift coefficients of 4.8 to be developed. In addition to presenting the description of the suction hole distribution and computed values of the suction velocity distribution, comparisons are made between the measured boundary-layer characteristics and one empirical, turbulent-boundary-layer profile description. The large influence of suction velocity on the wall shear stress is shown through the use of the momentum integral equation.

TABLE OF CONTENTS

LIST OF ILLUSTRATIONS

LIST OF TABLES

UNCLASSIFIED

Security Classification

DOCUMENT CONTROL DATA - R & D

(Security classification of title, body of abstract and indexing annotation must be entered when the overall report is classified)

1. ORIGINATING ACTIVITY (Corporate author)	2a. REPORT SECURITY CLASSIFICATION
Mississippi State University Department of Aerophysics and Aerospace Engineering State College, Mississippi	Unclassified 2b. GROUP

3. REPORT TITLE

INVESTIGATION OF THE SUCTION SYSTEM AND BOUNDARY-LAYER CHARACTERISTICS ON A HIGH-LIFT, BLC L-19 TEST AIRCRAFT

4. DESCRIPTIVE NOTES (Type of report and inclusive dates)

Final Report

5. AUTHOR(S) (First name, middle initial, last name)

L. J. Mertaugh
S. Burt

6. REPORT DATE	7a. TOTAL NO. OF PAGES	7b. NO. OF REFS
May 1973	54	6

8a. CONTRACT OR GRANT NO	9a. ORIGINATOR'S REPORT NUMBER(S)
DAAJ02-67-C-0016 b. PROJECT NO c. TASK 1F162204A14234 d.	USAAMRDL Technical Report 73-2 9b. OTHER REPORT NO(S) (Any other numbers that may be assigned this report) AASE Report No. 72-70

10. DISTRIBUTION STATEMENT

Approved for public release; distribution unlimited.

11. SUPPLEMENTARY NOTES	12. SPONSORING MILITARY ACTIVITY
Reproduction in this document may be better studied on microfiche	Eustis Directorate U. S. Army Air Mobility R & D Laboratory Fort Eustis, Virginia

13. ABSTRACT

This report presents the results of a test program which was intended to document the boundary-layer control system characteristics of the high-lift L-19 aircraft. This aircraft incorporates a distributed-suction, turbulent-boundary-layer control system which allows trimmed lift coefficients of 4.8 to be developed. In addition to presenting the description of the suction hole distribution and computed values of the suction velocity distribution, comparisons are made between the measured boundary-layer characteristics and one empirical, turbulent-boundary-layer profile description. The large influence of suction velocity on the wall shear stress is shown through the use of the momentum integral equation.

DD FORM 1 NOV 68 1473 REPLACES DD FORM 1473, 1 JAN 64, WHICH IS OBSOLETE FOR ARMY USE.

UNCLASSIFIED

Security Classification

14. KEY WORDS	LINK A		LINK B		LINK C	
	ROLE	WT	ROLE	WT	ROLE	WT
Boundary Layer Control Suction STOL						

LIST OF SYMBOLS

A	integrated Universal Profile constant	feet
B	integrated Universal Profile constant	feet
G	integrated Universal Profile constant	feet
H_{12}	boundary-layer profile parameter [$H_{12} = (\delta_1/\delta_2)$]	
p	static pressure	pounds per square foot or inches of water
Q	volume rate of flow	cubic feet per minute
$R_{e\delta_2}$	Reynolds number based on the boundary-layer momentum thickness	
S_{le}	upper surface distance measured from the leading edge of the wing section	inches
U	velocity (outside of boundary layer)	feet per second
U_τ	friction velocity [$U_\tau = (\tau_w/\rho)^{1/2}$]	feet per second
U_W	law-of-the-wake profile velocity contribution	feet per second
u	velocity (within the boundary layer)	feet per second
v_s	suction velocity (positive into the surface)	feet per second
y	lateral distance, perpendicular to the aircraft plane of symmetry	inches or feet
z	distance perpendicular to the wing surface (positive away from the surface)	inches
α	Universal Profile parameter	
β	Universal Profile parameter	
γ	Universal Profile parameter	
δ	boundary-layer thickness (δ = z at u = 0.99U)	inches or feet
δ_1	boundary-layer displacement thickness (incompressible) [$\delta_1 = \int_o^\infty (1-u/U)dy$]	inches or feet

δ_2	boundary-layer momentum thickness (incompressible) [$\varepsilon_2 = \int_o^\infty (u/U)\ (1-(u/U)^2)dy$]	inches or feet
θ	empirical shear stress function	
ν	coefficient of kinematic viscosity	square feet per second
ρ	density	slugs per cubic feet
τ	shear stress	pounds per square foot
ϕ	empirical shear stress function	
ψ	empirical shear stress function	

SUBSCRIPTS

o	free stream (ambient)
w	conditions at the surface
std	standard sea level
iw	wing interior

INTRODUCTION

The analysis of the turbulent boundary layer is highly dependent on the use of empirical formulations and results. The theoretical treatment of this realm of fluid mechanics, although improved over the years, is completely inadequate for anything but the most idealized flow conditions. While the empirical analysis of the turbulent layer provides useful results for some practical situations, it suffers from the limited amount of test data available. In particular, experimental data obtained in strong adverse pressure gradients and under conditions of relatively large amounts of boundary-layer suction are very limited. The development of an efficient distributed-suction, turbulent-boundary-layer control system is significantly limited by this lack of test data.

The high-lift L-19 aircraft developed at Mississippi State University represents the only known operational aircraft that utilizes a distributed-suction, turbulent-boundary-layer control system. This aircraft provides a unique opportunity to obtain test data pertaining to the operation and performance of such a system and to provide much-needed turbulent-boundary-layer data under conditions of adverse pressure gradient and large amounts of boundary-layer suction.

The results presented in this report are intended to document the suction configuration presently installed on the high-lift L-19 aircraft and to provide data and analysis to verify the suitability of some of the presently used empirical relationships. The test results are for the full-flap configuration with the aircraft operating at the lowest equivalent airspeed for which consistent test results are obtainable (36 mph). The boundary-layer measurements and analysis were made at one spanwise station on the inboard, flapped wing panel. Chordwise locations from 10 to 70 percent of the wing chord were studied.

DESCRIPTION OF TEST EQUIPMENT

The high-lift L-19 aircraft is described in detail in Reference 1. Photographs of the test aircraft are shown in Figure 1. Briefly, the aircraft is a standard L-19 with modifications made to the wing and the empennage. The wing modifications include: (1) leading-edge changes to provide a spanwise-constant leading-edge radius of 1.8 inches; (2) a new flap which eliminates the flap slot, provides venting of the flap interior to the interior of the wing, and uses inboard and outboard end plates; (3) the installation of suction holes in the upper surface of the wing and flap; and (4) the installation in each wing of one axial flow blower, driven by a hydraulic motor, with the associated internal ducting and external fairings. The hydraulic pump, for the blower motors, is mounted to the accessory section of the Continental Motors O-470-11 engine. The empennage changes include increased vertical stabilizer and rudder area and elevator end plates. The rear window of the aircraft is also modified to reduce flow separation. The test aircraft gross weight was maintained at 2530 pounds for this test program. Standard aircraft instrumentation was used with the static-pressure-system position errors determined with a trailing static bomb. Calibration of all pertinent flight instruments was performed.

Wing porosity measurements were made with a portable blower, venturi and plenum box. The venturi and pressure measuring instruments were calibrated. A typical arrangement of the equipment used in measuring wing porosity is shown in Figure 2.

The boundary-layer control system blower output was measured by means of the pressure rake shown in Figure 3. The rake provided 20 total-pressure tubes and 16 static-pressure tubes. Pressure data were measured with a water manometer mounted at the observer's seat. Readings were recorded by marking the water column height on a clear plastic oversheet.

Wing static-pressure distribution data were obtained using plastic strip tubing bonded to the wing surface. One end of the tubing was sealed and one static-pressure tap hole was drilled into each tube at the desired chordwise locations. The remaining end of the strip tubing was connected to the water manometer. Pressure readings were recorded by the observer using the plastic oversheets.

The boundary-layer velocity profile measurements were obtained with a curved boundary-layer mouse. The mouse provided 16 total-pressure tubes and 1 static-pressure tube. The forward ends of the total-pressure tubes were flattened and ground to a height of 0.023 inch and a width of 0.052 inch. The internal height of the total-pressure tubes' opening was 0.006 inch. The boundary-layer mouse configuration is shown in Figure 4.

The mouse was taped to the wing surface and was connected to the water manometer by plastic strip tubing. The height of the total-pressure tubes above the wing surface was determined by photographing the mouse with a 0.001-inch scale positioned alongside at each chordwise position tested. Because the mouse static-pressure tube was found to give inconsistent readings due to problems with tube alignment, the static-pressure measurements used with the mouse data were obtained with externally mounted "flush" static-pressure taps. These taps consisted of three layers of laminated brass shim stock. The middle layer was cut out to form a plenum, and the static-pressure tap was drilled in the outer layer. A small length of stainless steel tubing was soldered to one end to connect the plenum to the plastic tubing. One of these tabs was bonded to the wing surface on each side of the mouse. The total thickness of the tap was approximately 0.020 inch with a width of 0.5 inch and a length of 1.5 inches. Tests were conducted on the wing of a glider, and the static pressure obtained with this device was found to agree with the data obtained using the plastic strip tubing within the accuracy of reading the water manometer.

DATA REDUCTION

The porosity data presented in this report are given in terms of "equivalent" flow rate as a function of differential pressure. The porosity measurements were made under conditions that were approximately equal to standard sea level conditions so that the volume flow rate can be considered to be valid for standard conditions. Variations in atmospheric conditions that existed during the porosity measurements represented variations in $\sqrt{\rho_{std}/\rho}$ of less than ± 2 percent, which was well within the scatter of the test data. The corresponding value for flow rate at a given value of differential pressure for conditions other than standard is obtained by ratioing the flow rate obtained from the figures by the square root of the density ratio (i.e., $Q = Q_{std} \sqrt{\rho_{std}/\rho}$).

The suction velocities determined from the porosity measurements were obtained by dividing the flow rate corresponding to a given row of suction holes by the effective wing surface area associated with that row. The effective area was defined as the product of the distance between lines halfway between the adjacent rows of suction holes and the reference span of the suction hole row. The reference span was 1 foot. On the average, there were 116 suction holes in 1 foot of row span. The porosity data were corrected to 116 holes when a different number of holes were found in the row of holes being tested. The number of holes per foot of span varied between 110 and 124 for the different locations tested. The values of suction velocity used in the boundary-layer analysis were converted to true velocity by multiplying by the square root of the density ratio corresponding to the flight test conditions.

The manometer board used for pressure measurements was leveled prior to recording the test data, and a factor of 5.2022 was used to convert from inches of water to pounds per square foot.

RESULTS AND DISCUSSION

SUCTION HOLE DISTRIBUTION

The high-lift L-19 aircraft represents a number of years of trial-and-error experimentation which has resulted in an aircraft that develops a maximum trimmed lift coefficient of 4.8 with reasonable stall characteristics, except for the lack of adequate stall warning, and moderate amounts of stability and control in the slow flight regime. In addition to the obvious changes in the aircraft configuration described earlier in this report, the suction hole distribution presently employed is the result of a number of changes to the originally computed distribution. Only limited records were maintained regarding these changes to the suction hole distribution. The desire to document the present distribution required that new measurements be made. For measurement purposes, the identification of the hole sizes was based on the three sizes of holes (0.018-, 0.024- and 0.028-inch diameter) used in the initial drilling. The results of the present measurements did not indicate any consistent trend to imply hole diameters other than the three specified sizes, but there was random variation indicating that the hole obtained from a given drill was not as consistent as would be desired. The wing span was divided into 12 measurement stations with the rows of suction holes being reasonably consistent between each station. Local concentrations of suction holes, in the neighborhood of areas of the skin where internal brackets, etc., prevented the installation of suction holes, were neglected. These areas represent less than 5 percent of the sucked area of the wing. The distribution of suction holes defined at a given spanwise station represents the rows of holes between that station and the next inboard station for which a hole distribution is given. Measurements were made only on the left wing, but symmetry is assumed. The distribution of suction holes is given as a function of the spanwise distance aft of the wing leading edge in Tables I through XII. The hole distributions represent the wing with full flap deflection. For the flapped span of the wing, the fixed upper skin extends back to a surface distance of 53.50 inches. When the flap is retracted to the zero deflection position, the upper surface distance is reduced by 6.6 inches and 14 rows of suction holes are covered by the upper, fixed-wing surface.

POROSITY MEASUREMENTS

A number of different arrangements were tried in measuring the porosity of the drilled suction holes on the wing skin. Initial efforts used a

TABLE I. SUCTION HOLE GEOMETRY, STA = 64.5

Row	Diameter (in.)	S_{le} (in.)	Row	Diameter (in.)	S_{le} (in.)
1	.028	5.80	51	.018	37.27
2	.028	6.06	52	.018	37.84
3	.028	6.33	53	.018	38.44
4	.028	6.61	54	.018	39.08
5	.028	6.81	55	.018	39.59
6	.028	7.13	56	.018	40.47
7	.028	7.47	57	.018	40.84
8	.028	7.84	58	.018	41.55
9	.028	8.20	59	.018	42.20
10	.028	8.61	60	.018	44.23
11	.028	8.95	61	.018	45.00
12	.028	9.42	62	.018	45.66
13	.028	9.89	63	.018	46.36
14	.028	13.88	64	.018	47.02
15	.018	14.33	65	.018	47.64
16	.024	14.80	66	.018	48.91
17	.018	15.39	67	.018	49.59
18	.024	15.81	68	.018	50.30
19	.018	16.41	69	.018	51.03
20	.024	16.99	70	.018	51.69
21	.018	17.47	71	.018	53.83
22	.024	17.98	72	.018	54.66
23	.024	18.80	73	.018	54.88
24	.024	19.75	74	.018	55.38
25	.018	20.19	75	.018	55.86
26	.018	20.53	76	.018	56.44
27	.018	21.02	77	.018	56.92
28	.018	21.48	78	.018	57.38
29	.018	22.03	79	.018	57.88
30	.018	22.53	80	.018	58.38
31	.018	23.05	81	.018	58.88
32	.018	23.63	82	.018	59.03
33	.018	24.27	83	.018	59.84
34	.018	24.78	84	.018	60.31
35	.018	25.41	85	.018	61.39
36	.018	25.99	86	.018	61.88
37	.018	26.91	87	.018	62.38
38	.018	28.05	88	.018	62.84
39	.018	28.36	89	.018	63.34
40	.018	29.44	90	.018	64.34
41	.018	30.13	91	.018	65.38
42	.018	30.89	92	.018	66.34
43	.018	31.59	93	.018	67.34
44	.018	32.34	94	.018	68.25
45	.018	33.03	95	.018	69.27
46	.018	33.47	96	.018	70.28
47	.018	33.99	97	.018	71.31
48	.018	34.95	98	.018	72.31
49	.018	36.09	T.E.	-	74.47
50	.018	36.72			

TABLE II. SUCTION HOLE GEOMETRY, STA = 57.5

Row	Diameter (in.)	S_{le} (in.)	Row	Diameter (in.)	S_{le} (in.)
1	.028	5.83	63	.024	31.31
2	.028	6.09	64	.018	31.69
3	.028	6.17	65	.024	32.00
4	.028	6.63	66	.018	32.38
5	.028	6.84	67	.024	32.63
6	.028	7.16	68	.024	33.09
7	.028	7.47	69	.018	33.59
8	.028	7.86	70	.018	34.03
9	.028	8.23	71	.024	34.95
10	.028	8.66	72	.018	36.16
11	.028	8.98	73	.018	36.81
12	.028	9.50	74	.018	37.36
13	.028	9.92	75	.018	37.95
14	.028	13.63	76	.018	38.50
15	.028	13.97	77	.018	39.13
16	.018	14.38	78	.018	39.66
17	.024	14.64	79	.018	40.30
18	.024	14.88	80	.018	40.94
19	.024	15.13	81	.018	41.61
20	.018	15.39	82	.018	42.27
21	.024	15.63	83	.018	44.28
22	.024	15.89	84	.018	44.66
23	.024	16.19	85	.018	45.03
24	.018	16.44	86	.018	45.69
25	.024	16.72	87	.018	46.39
26	.024	17.06	88	.018	47.03
27	.024	17.28	89	.018	47.69
28	.018	17.59	90	.018	49.97
29	.024	18.06	91	.018	49.69
30	.024	18.98	92	.018	50.34
31	.024	19.83	93	.018	51.09
32	.024	20.00	94	.018	51.75
33	.018	20.22	95	.018	53.88
34	.018	20.63	96	.018	54.44
35	.024	20.91	97	.018	54.94
36	.018	21.06	98	.018	55.44
37	.018	21.56	99	.018	55.97
38	.024	21.78	100	.018	56.47
39	.018	22.06	101	.018	57.03
40	.018	22.61	102	.018	57.44
41	.024	22.88	103	.018	58.00
42	.018	23.13	104	.018	58.41
43	.024	23.41	105	.018	58.95
44	.018	23.73	106	.018	59.27
45	.024	24.05	107	.018	59.88
46	.018	24.31	108	.018	60.44
47	.024	24.56	109	.018	61.42
48	.018	24.86	110	.018	61.97
49	.024	25.14	111	.018	62.39
50	.018	25.59	112	.018	62.88
51	.024	25.72	113	.018	63.42
52	.018	26.00	114	.018	64.44
53	.018	26.88	115	.018	65.44
54	.018	28.09	116	.018	66.42
55	.024	28.47	117	.018	67.41
56	.024	28.72	118	.018	68.38
57	.024	29.19	119	.018	69.34
58	.018	29.52	120	.018	70.34
59	.024	29.91	121	.018	71.38
60	.018	30.22	122	.018	72.41
61	.018	30.56	T.E.	-	74.56
62	.018	31.00			

TABLE III. SUCTION HOLE GEOMETRY, STA = 71.2

Row	Diameter (in.)	S_{le} (in.)	Row	Diameter (in.)	S_{le} (in.)
1	.028	5.84	64	.018	31.66
2	.028	6.09	65	.024	32.03
3	.028	6.33	66	.018	32.44
4	.028	6.63	67	.024	32.77
5	.028	6.84	68	.018	33.13
6	.028	7.16	69	.018	33.69
7	.028	7.47	70	.018	34.28
8	.028	7.84	71	.018	35.53
9	.028	8.22	72	.018	35.97
10	.028	8.66	73	.018	36.44
11	.028	8.98	74	.018	36.86
12	.028	9.48	75	.018	37.36
13	.028	9.91	76	.018	37.91
14	.028	13.59	77	.018	38.50
15	.024	13.87	78	.018	39.13
16	.024	14.47	79	.018	39.72
17	.024	14.66	80	.018	40.31
18	.024	14.92	81	.018	40.97
19	.024	15.19	82	.018	41.63
20	.024	15.44	83	.018	42.28
21	.024	15.66	84	.018	43.72
22	.024	15.91	85	.018	44.36
23	.024	16.20	86	.018	44.69
24	.024	16.50	87	.018	44.97
25	.024	16.75	88	.018	45.69
26	.024	17.08	89	.018	46.38
27	.024	17.30	90	.018	47.11
28	.024	17.72	91	.018	47.69
29	.024	18.00	92	.018	49.00
30	.024	18.34	93	.018	49.63
31	.024	19.78	94	.018	50.38
32	.024	20.00	95	.018	51.09
33	.018	20.23	96	.018	51.72
34	.018	20.63	97	.018	53.47
35	.024	20.84	98	.018	53.91
36	.018	21.09	99	.018	54.47
37	.018	21.58	100	.018	54.97
38	.024	21.81	101	.018	55.44
39	.018	22.09	102	.018	56.00
40	.018	22.61	103	.018	56.50
41	.024	22.88	104	.018	57.06
42	.018	23.17	105	.018	57.47
43	.024	23.47	106	.018	58.03
44	.018	23.80	107	.018	58.47
45	.024	24.03	108	.018	58.97
46	.018	24.31	109	.018	59.44
47	.024	24.58	110	.018	59.98
48	.018	24.88	111	.018	60.41
49	.024	25.17	112	.018	61.47
50	.018	25.48	113	.018	62.00
51	.024	25.83	114	.018	62.41
52	.018	26.06	115	.018	62.84
53	.018	27.50	116	.018	63.41
54	.018	28.11	117	.018	64.41
55	.024	28.44	118	.018	65.47
56	.018	28.81	119	.018	66.41
57	.024	29.22	120	.018	67.41
58	.018	29.55	121	.018	68.38
59	.024	29.92	122	.018	69.38
60	.018	30.25	123	.018	70.38
61	.024	30.63	124	.018	71.41
62	.018	31.06	125	.018	72.41
63	.024	31.34	T.E.	-	74.56

TABLE IV. SUCTION HOLE GEOMETRY, STA = 85.4

Row	Diameter (in.)	S_{le} (in.)	Row	Diameter (in.)	S_{le} (in.)
1	.028	5.81	64	.018	32.09
2	.028	6.06	65	.018	32.41
3	.028	6.31	66	.018	32.81
4	.028	6.59	67	.018	33.16
5	.028	6.81	68	.018	33.75
6	.028	7.13	69	.018	34.31
7	.028	7.44	70	.018	35.56
8	.028	7.81	71	.018	36.00
9	.028	8.19	72	.018	36.47
10	.028	8.63	73	.018	36.88
11	.028	8.94	74	.018	37.38
12	.028	9.44	75	.018	38.00
13	.028	9.91	76	.018	38.53
14	.018	13.63	77	.018	39.13
15	.024	14.02	78	.018	39.72
16	.024	14.48	79	.018	40.34
17	.018	14.69	80	.018	41.00
18	.018	15.00	81	.018	41.63
19	.018	15.25	82	.018	42.28
20	.024	15.47	83	.018	43.75
21	.018	15.72	84	.018	44.38
22	.024	16.00	85	.018	44.63
23	.018	16.31	86	.018	45.00
24	.024	16.50	87	.018	45.81
25	.018	16.78	88	.018	46.38
26	.024	17.09	89	.018	47.09
27	.018	17.38	90	.018	47.69
28	.024	17.69	91	.018	49.03
29	.018	18.00	92	.018	49.66
30	.024	18.36	93	.018	50.34
31	.024	19.81	94	.018	51.14
32	.018	20.00	95	.018	51.67
33	.024	20.22	96	.018	53.50
34	.018	20.67	97	.018	53.88
35	.018	20.88	98	.018	54.50
36	.024	21.13	99	.018	54.89
37	.018	21.63	100	.018	55.50
38	.018	21.84	101	.018	55.89
39	.024	22.13	102	.018	56.50
40	.018	22.66	103	.018	57.05
41	.018	22.91	104	.018	57.50
42	.024	23.19	105	.018	58.05
43	.018	23.91	106	.018	58.44
44	.018	24.13	107	.018	59.02
45	.024	24.41	108	.018	59.44
46	.018	24.64	109	.018	59.88
47	.018	24.94	110	.018	60.44
48	.018	25.27	111	.018	61.47
49	.024	25.56	112	.018	62.00
50	.018	25.81	113	.018	62.44
51	.018	26.13	114	.018	62.88
52	.018	27.61	115	.018	63.44
53	.024	28.16	116	.018	64.44
54	.018	28.48	117	.018	65.47
55	.018	28.84	118	.018	66.44
56	.018	29.25	119	.018	67.47
57	.024	29.59	120	.018	68.38
58	.018	29.97	121	.018	69.38
59	.018	30.28	122	.018	70.38
60	.018	30.75	123	.018	71.41
61	.024	31.09	124	.018	72.44
62	.018	31.41	T.E.	-	74.56
63	.018	31.72			

TABLE V. SUCTION HOLE GEOMETRY, STA = 93.1

Row	Diameter (in.)	S_{le} (in.)	Row	Diameter (in.)	S_{le} (in.)
1	.028	5.81	63	.018	32.17
2	.028	6.06	64	.018	32.52
3	.028	6.31	65	.018	32.88
4	.028	6.63	66	.018	33.13
5	.028	6.81	67	.018	33.75
6	.028	7.13	68	.018	34.38
7	.028	7.44	69	.018	35.59
8	.028	7.84	70	.018	36.06
9	.028	8.28	71	.018	36.49
10	.028	8.63	72	.018	36.94
11	.028	8.97	73	.018	37.38
12	.028	9.44	74	.018	38.03
13	.028	9.91	75	.018	38.61
14	.018	13.59	76	.018	39.19
15	.018	14.00	77	.018	39.75
16	.024	14.63	78	.018	40.38
17	.018	14.88	79	.018	41.14
18	.024	15.09	80	.018	41.69
19	.018	15.28	81	.018	42.31
20	.018	15.59	82	.018	43.77
21	.018	15.81	83	.018	44.38
22	.024	16.13	84	.018	44.64
23	.018	16.34	85	.018	45.03
24	.018	16.63	86	.018	45.66
25	.018	16.88	87	.018	46.34
26	.024	17.09	88	.018	47.09
27	.018	17.38	89	.018	47.72
28	.018	17.66	90	.018	49.05
29	.024	18.03	91	.018	49.69
30	.018	18.47	92	.018	50.38
31	.018	19.88	93	.018	51.08
32	.018	20.16	94	.018	51.77
33	.024	20.47	95	.018	53.53
34	.018	21.00	96	.018	53.95
35	.018	21.28	97	.018	54.53
36	.024	21.59	98	.018	55.00
37	.018	22.19	99	.018	55.53
38	.018	22.50	100	.018	56.02
39	.024	22.84	101	.018	56.56
40	.018	23.44	102	.018	57.08
41	.018	23.72	103	.018	57.55
42	.024	24.08	104	.018	58.08
43	.018	24.38	105	.018	58.53
44	.018	24.72	106	.018	59.05
45	.018	25.09	107	.018	59.47
46	.024	25.41	108	.018	59.88
47	.018	25.73	109	.018	60.50
48	.018	26.06	110	.018	61.50
49	.018	27.75	111	.018	62.03
50	.024	28.19	112	.018	62.47
51	.018	28.44	113	.018	62.89
52	.018	28.67	114	.018	63.44
53	.018	28.98	115	.018	64.44
54	.024	29.11	116	.018	65.50
55	.018	29.53	117	.018	66.45
56	.018	29.84	118	.018	67.45
57	.018	30.19	119	.018	68.44
58	.024	30.50	120	.018	69.39
59	.018	30.84	121	.018	70.41
60	.018	31.13	122	.018	71.41
61	.018	31.53	123	.018	72.47
62	.024	31.81	T.E.	-	74.59

TABLE VI. SUCTION HOLE GEOMETRY, STA = 99.9

Row	Diameter (in.)	S_{le} (in.)	Row	Diameter (in.)	S_{le} (in.)
1	.028	5.81	50	.018	38.66
2	.028	6.08	51	.018	39.22
3	.028	6.34	52	.018	39.78
4	.028	6.63	53	.018	40.44
5	.028	6.84	54	.018	41.16
6	.028	7.16	55	.018	41.75
7	.028	7.47	56	.018	42.38
8	.028	7.86	57	.018	43.81
9	.028	8.28	58	.018	44.41
10	.028	8.66	59	.018	45.08
11	.028	8.98	60	.018	45.83
12	.028	9.47	61	.018	46.41
13	.028	9.91	62	.018	47.13
14	.018	14.69	63	.018	47.75
15	.024	15.16	64	.018	49.09
16	.018	15.63	65	.018	49.72
17	.028	16.17	66	.018	50.41
18	.018	16.64	67	.018	51.13
19	.024	17.17	68	.018	51.77
20	.018	17.72	69	.018	53.61
21	.024	18.13	70	.018	54.03
22	.018	18.53	71	.018	54.59
23	.018	19.89	72	.018	55.06
24	.024	20.52	73	.018	55.56
25	.018	21.06	74	.018	56.06
26	.024	21.69	75	.018	56.59
27	.018	22.25	76	.018	57.13
28	.024	22.91	77	.018	57.56
29	.018	23.47	78	.018	58.13
30	.024	24.16	79	.018	58.56
31	.018	24.66	80	.018	59.09
32	.024	25.47	81	.018	59.52
33	.018	26.13	82	.018	59.89
34	.018	27.81	83	.018	60.52
35	.024	28.25	84	.018	61.56
36	.018	28.72	85	.018	62.06
37	.024	29.28	86	.018	62.52
38	.018	29.88	87	.018	62.94
39	.024	30.56	88	.018	63.50
40	.018	31.19	89	.018	64.50
41	.024	31.88	90	.018	65.56
42	.018	32.59	91	.018	66.53
43	.018	33.13	92	.018	67.50
44	.018	33.78	93	.018	68.47
45	.018	34.44	94	.018	69.44
46	.018	35.66	95	.018	70.50
47	.018	36.50	96	.018	71.44
48	.018	37.44	97	.018	72.50
49	.018	38.06	T.E.	-	74.63

TABLE VII. SUCTION HOLE GEOMETRY, STA = 116.4

Row	Diameter (in.)	S_{le} (in.)	Row	Diameter (in.)	S_{le} (in.)
1	.028	5.22	51	.018	37.31
2	.028	5.47	52	.018	37.94
3	.028	5.75	53	.018	38.41
4	.028	5.97	54	.018	39.02
5	.028	6.25	55	.018	39.72
6	.028	6.53	56	018	40.47
7	.028	6.91	57	.018	41.05
8	.028	7.25	58	.018	41.61
9	.028	7.59	59	.018	42.30
10	.028	8.00	60	.018	43.05
11	.028	8.34	61	.018	43.66
12	.028	8.75	62	.018	44.31
13	.028	9.13	63	.018	44.91
14	.028	9.53	64	.018	45.63
15	.024	13.94	65	.018	46.31
16	.024	14.41	66	.018	46.97
17	.018	14.88	67	.018	48.28
18	.024	15.41	68	.018	48.97
19	.018	15.88	69	.018	49.63
20	.024	16.44	70	.018	50.38
21	.018	16.97	71	.018	50.97
22	.024	17.39	72	.018	52.75
23	.018	17.78	73	.018	53.28
24	.018	19.22	74	.018	53.81
25	.024	19.78	75	018	54.22
26	.018	20.31	76	.018	54.75
27	.024	20.94	77	.018	55.25
28	.018	21.50	78	.018	55.75
29	.024	22.16	79	.018	56.31
30	.018	22.50	80	.018	56.75
31	.024	23.42	81	.018	57.25
32	.018	24.03	82	.018	57.72
33	.024	24.66	83	.018	58.25
34	.018	25.38	84	.018	58.78
35	.018	27.13	85	.018	59.25
36	.024	27.44	86	.018	59.81
37	.018	28.00	87	.018	60.88
38	.024	28.53	88	.018	61.31
39	.018	29.14	89	.018	61.81
40	.024	29.78	90	.018	62.31
41	.018	30.47	91	.018	62.81
42	.024	31.14	92	.018	63.92
43	.018	31.88	93	.018	64.88
44	.018	32.31	94	.018	65.92
45	.018	33.00	95	.018	66.78
46	.018	33.67	96	.018	67.78
47	.018	34.25	97	.018	68.75
48	.018	34.94	98	.018	69.75
49	.018	35.69	99	.018	70.75
50	.018	36.75	100	.018	71.75
			T.E.		72.38

TABLE VIII. SUCTION HOLE GEOMETRY, STA = 135.9

Row	Diameter (in.)	S_{le} (in.)	Row	Diameter (in.)	S_{le} (in.)
1	.024	5.09	35	.018	27.63
2	.024	5.41	36	.024	28.34
3	.024	5.66	37	.018	28.98
4	.024	5.91	38	.024	29.63
5	.024	6.19	39	.018	30.19
6	.024	6.44	40	.024	30.72
7	.024	6.78	41	.018	31.23
8	.024	7.09	42	.018	32.44
9	.024	7.47	43	.018	33.05
10	.024	7.84	44	.024	33.59
11	.024	8.16	45	.013	34.09
12	.024	8.47	46	.024	34.44
13	.024	8.86	47	.018	35.05
14	.024	9.22	48	.024	35.50
15	.018	13.48	49	.018	36.05
16	.018	13.91	50	.024	36.63
17	.018	14.33	51	.018	37.16
18	.024	14.75	52	.018	38.19
19	.018	15.22	53	.018	39.66
20	.024	15.66	54	.018	40.58
21	.018	16.13	55	.024	41.19
22	.024	16.55	56	.018	41.81
23	.018	16.91	57	.024	42.50
24	.018	18.34	58	.018	43.14
25	.018	19.14	59	.024	43.84
26	.024	19.88	60	.018	44.53
27	.018	20.64	61	.024	45.22
28	.024	21.38	62	.018	45.78
29	.018	22.14	63	.024	46.44
30	.024	22.84	64	.018	47.09
31	.018	23.55	65	.024	47.75
32	.018	25.25	66	.018	48.47
33	.018	26.31	67	.018	49.36
34	.024	26.97	T.E.	-	60.50

TABLE IX. SUCTION HOLE GEOMETRY, STA = 153.9

Row	Diameter (in.)	S_{le} (in.)	Row	Diameter (in.)	S_{le} (in.)
1	.024	4.98	35	.018	26.25
2	.024	5.25	36	.024	26.88
3	.024	5.53	37	.018	27.47
4	.024	5.78	38	.024	28.00
5	.024	6.06	39	.018	28.66
6	.024	6.31	40	.024	29.16
7	.024	6.63	41	.018	29.63
8	.024	6.89	42	.018	30.83
9	.024	7.25	43	.018	31.36
10	.024	7.56	44	.024	31.84
11	.024	7.88	45	.018	32.31
12	.024	8.16	46	.024	32.75
13	.024	8.50	47	.018	33.19
14	.024	8.81	48	.024	33.63
15	.018	13.03	49	.018	34.16
16	.018	13.41	50	.024	34.63
17	.018	13.81	51	.018	35.13
18	.024	14.19	52	.018	36.09
19	.018	14.58	53	.018	37.56
20	.024	14.95	54	.018	38.34
21	.018	15.30	55	.024	38.91
22	.024	15.69	56	.018	39.44
23	.018	16.06	57	.024	40.03
24	.018	17.50	58	.018	40.56
25	.018	18.22	59	.024	41.16
26	.024	18.92	60	.018	41.75
27	.018	19.63	61	.024	42.34
28	.024	20.34	62	.018	42.88
29	.018	21.02	63	.024	43.47
30	.024	21.70	64	.018	44.09
31	.018	22.34	65	.024	44.63
32	.018	24.00	66	.018	45.22
33	.018	24.98	67	.018	46.16
34	.024	25.63	T.E.	-	57.25

TABLE X. SUCTION HOLE GEOMETRY, STA = 171.9

Row	Diameter (in.)	S_{le} (in.)	Row	Diameter (in.)	S_{le} (in.)
1	.028	4.75	35	.018	24.77
2	.028	5.06	36	.024	25.38
3	.028	5.31	37	.018	25.91
4	.028	5.59	38	.024	26.44
5	.028	5.88	39	.018	27.06
6	.028	6.09	40	.024	27.50
7	.028	6.38	41	.018	27.98
8	.028	6.64	42	.018	29.17
9	.028	6.94	43	.018	29.63
10	.028	7.22	44	.024	30.06
11	.028	7.52	45	.018	30.47
12	.028	7.77	46	.024	30.84
13	.028	8.06	47	.018	31.28
14	.028	8.36	48	.024	31.69
15	.018	12.50	49	.018	32.19
16	.018	12.88	50	.024	32.63
17	.018	13.22	51	.018	33.03
18	.024	13.53	52	.018	34.97
19	.018	13.84	53	.018	35.91
20	.024	14.16	54	.018	36.09
21	.018	14.44	55	.024	36.56
22	.024	14.78	56	.018	37.03
23	.018	15.16	57	.024	37.50
24	.018	16.56	58	.018	37.97
25	.018	17.25	59	.024	38.41
26	.024	17.91	60	.018	38.88
27	.018	18.56	61	.024	39.47
28	.024	19.22	62	.018	39.92
29	.018	19.84	63	.024	40.50
30	.024	20.44	64	.018	41.00
31	.018	21.06	65	.024	41.41
32	.018	22.66	66	.018	41.88
33	.018	23.63	67	.018	42.88
34	.024	24.19	T.E.	-	53.88

TABLE XI. SUCTION HOLE GEOMETRY, STA = 189.9

Row	Diameter (in.)	S_{le} (in.)	Row	Diameter (in.)	S_{le} (in.)
1	.024	4.63	24	.018	19.83
2	.024	4.88	25	.018	21.38
3	.024	5.16	26	.018	22.28
4	.024	5.42	27	.018	23.38
5	.024	5.64	28	.018	24.41
6	.024	5.89	29	.018	25.48
7	.024	6.16	30	.018	26.41
8	.024	6.41	31	.018	27.53
9	.024	6.64	32	.018	27.88
10	.024	6.95	33	.018	28.66
11	.024	7.19	34	.018	29.41
12	.024	7.41	35	.018	30.28
13	.024	7.66	36	.018	31.05
14	.024	7.91	37	.018	31.86
15	.018	12.00	38	.018	33.27
16	.018	12.63	39	.018	33.84
17	.018	13.19	40	.018	34.66
18	.018	13.78	41	.018	35.34
19	.018	14.34	42	.018	36.09
20	.018	15.63	43	.018	36.97
21	.018	16.56	44	.018	37.94
22	.018	17.53	45	.018	38.63
23	.018	18.72	46	.018	39.66
			T.E.	-	50.88

TABLE XII. SUCTION HOLE GEOMETRY, STA = 206.4

Row	Diameter (in.)	S_{le} (in.)	Row	Diameter (in.)	S_{le} (in.)
1	.024	4.17	24	.018	18.47
2	.024	4.44	25	.018	20.05
3	.024	4.72	26	.018	20.81
4	.024	5.00	27	.018	21.83
5	.024	5.28	28	.018	22.75
6	.024	5.34	29	.018	23.75
7	.024	5.77	30	.018	24.66
8	.024	5.94	31	.018	25.72
9	.024	6.19	32	.018	26.03
10	.024	6.39	33	.018	26.75
11	.024	6.64	34	.018	27.47
12	.024	6.88	35	.018	28.22
13	.024	7.06	36	.018	28.94
14	.024	7.27	37	.018	29.67
15	.018	11.31	38	.018	31.00
16	.018	11.88	39	.018	31.47
17	.018	12.38	40	.018	32.28
18	.018	12.91	41	.018	32.69
19	.018	13.44	42	.018	33.22
20	.018	14.58	43	.018	33.98
21	.018	15.23	44	.018	34.83
22	.018	16.38	45	.018	35.31
23	.018	17.41	46	.018	36.38
			T.E.	-	47.25

plenum box which covered a 12-inch by 12-inch area of the skin. The variation in hole size sometimes found with adjacent rows of suction holes made these data difficult to work with. The data presented in this report were obtained with a plenum box that covered a 1-foot length of only one row of suction holes. Although tests on suction holes drilled in materials other than metal have shown a difference in porosity depending on the direction of flow through the holes, measurements made with the present equipment, both blowing and sucking, show little difference in the flow rate with flow direction for a given pressure differential across the aluminum skin. All of the present porosity data were measured with the flow passing from the interior of the wing out into the plenum. While the direction of the flow is known to make little difference for measurements made on the wing skin, the possible error in the measured porosity of the suction holes on the flap surface is unknown. The flap is constructed of wood with plywood skins of about 0.030 inch thickness. A few porosity measurements were made by mounting the plenum and venturi on the wing while using the aircraft boundary-layer control system blowers to provide the pressure differential across the skin. Although the range of differential pressures was limited with this arrangement, the data did agree with the measurements obtained with the external suction source. Most of the porosity measurements were made on the inboard portion of the wing. The data are considered, however, to be representative of all of the suction holes.

Selected porosity measurements for the three hole sizes are shown in Figures 5, 6 and 7. The number of data shown in these figures has been minimized for clarity, but the selected data do represent the extremes of porosity measured for each hole size. The curves shown in Figures 5 and 6 are the least-squares fit to a power curve based on all of the obtained test data. Two curves are shown for the 0.018-inch holes in Figure 5 because the measured porosity of the flap was consistently higher than the porosity of the same size holes on the aluminum skin of the wing. These faired curves are the porosity characteristics used in the determination of the suction velocity distributions discussed in subsequent portions of this report. The solid curve shown in Figure 7 represents the porosity characteristics used in computing the suction velocities for the 0.028-inch holes. The dashed curve is the correct least-squares fit to the test data. The solid curve resulted from an error in converting the units of the measured data, but the small difference between the two curves did not justify recomputing the suction velocities and revising the resulting analysis.

SUCTION VELOCITY DATA

The static-pressure data used in computing the suction velocities are presented in Figure 8 for the four spanwise stations of interest with full flaps and an equivalent airspeed of 36 miles per hour.

The computed equivalent suction velocity distributions for the full flap configuration at an equivalent airspeed of 36 miles per hour and an internal wing pressure of 58.27 pounds per square foot below ambient pressure are shown in Figures 9 through 12 for four spanwise stations as a function of surface distance aft of the wing leading edge. The curves shown on these figures represent an effective continuous distribution that averages the abrupt changes in computed suction velocity due to changes in hole size between adjacent rows of suction holes. The curves have been adjusted to give the same total flow as the sum of the flow rates computed for each row of holes. The curve shown in Figure 9 was used for the boundary-layer analysis. Changes in equivalent airspeed and/or aircraft weight would change the chordwise pressure distributions and the resulting distribution of suction velocities.

The total equivalent flow rate obtained by integrating the computed suction velocities (using the data of Figures 9 through 12) over the wing of the L-19 aircraft was found to be 9,770 cubic feet per minute. The spanwise distribution of suction flow rate was based on the computed flow rate at the four spanwise stations and the measured spanwise suction hole area distribution. This method of interpolating between the computed values obviously neglects the fact that the flow coefficients for the different hole sizes are not the same, but this approach provided a relatively simple method that agreed well with the relative magnitudes of the four computed values of suction flow rate. The resulting spanwise distribution of suction flow rate is shown in Figure 13.

The internal wing pressure of -58.27 pounds per square foot, used in the above calculations, was the value measured at a location midway to the left wing tip. This pressure is representative of the average internal wing pressure where values of as low as -52.54 pounds per square foot were noted at the wing tip in an earlier test program. The internal wing pressures measured in the right wing tended to be about 2.6 pounds per square foot lower (less negative) than those found in the left wing. Calculations assuming a constant internal wing pressure of -52.02 pounds per square foot yielded a total equivalent suction flow rate of 9,080 cubic feet per minute. The uncertainty in computing suction flow due to the possible variation in internal wing pressure (9,080 to 9,770 cubic feet per minute) is considered to be within the accuracy of the assumed porosity characteristics.

The boundary-layer control system blower output was measured to be 8,620 cubic feet per minute (equivalent flow rate) in flight. This value was based on the data obtained with the pressure rake mounted on the outlet of the left wing blower. The right wing blower output was assumed to be the same as the left wing blower output. Although the agreement between the measured blower output and the integrated computed suction velocities is not as close as is desired, it is considered to be reasonable in light of the various assumptions, approximations and measurement accuracies that were involved in arriving at these values.

BOUNDARY-LAYER CHARACTERISTICS

The measured boundary-layer velocity ratio profiles obtained on the L-19 wing at an equivalent airspeed of 36 miles per hour and with full flap deflection are shown in Figure 14. The profiles were obtained at a distance of 44.5 inches outboard of the aircraft centerline and surface distances (aft of the wing leading edge) of 8.38, 11.75, 21.57, 34.79, 41.19 and 47.72 inches. These distances correspond to 10.0, 15.0, 30.0, 50.0, 60.0 and 70.0 percent wing chord, respectively. The faired velocity profiles used in the boundary-layer analysis are indicated by the solid curves.

As was noted in the Introduction section, the bulk of useful turbulent-boundary-layer theory is based on empirical results. Most of the turbulent-boundary-layer analyses are dependent upon the use of some form of multiparameter velocity profile definition. The work of Coles (see Reference 2) is a much-used representation which includes the "law of the wall" and "law of the wake" expressions. Similar descriptions of the turbulent-boundary-layer velocity profile, considering suction or injection at the wall, were presented by Black and Sarnecki (Reference 3) and Cornish (Reference 4). A comparison of one of these so-called Universal Turbulent Boundary-Layer Velocity Profiles with the measured test data is also shown in Figure 14. Cornish's profile representation was used since it is slightly more recent than Reference 3 and does consider suction, which is not introduced in Reference 2.

The Universal Velocity Profile is based on the equation

$$(u-U)/U_\tau = (1-v_s U/U_\tau^2)^{1/2}\,\alpha + (U_w/U_\tau)\beta - (v_s/U_\tau)\gamma \qquad (1)$$

where α, β and γ are universal functions of the height parameter (z/δ); they are given in table form in Reference 4 and are repeated below for convenience.

z/δ	α	β	γ
0.00	-	1.00	-
0.01	-11.20	-1.00	31.36
0.02	-9.52	-1.00	22.50
0.05	-7.28	-0.99	13.30
0.10	-5.60	-0.97	7.84
0.20	-3.86	-0.90	3.78
0.30	-2.74	-0.79	2.15
0.40	-1.99	-0.65	1.24
0.50	-1.39	-0.50	0.71

z/δ	α	β	γ
0.60	-0.94	-0.35	0.38
0.70	-0.58	-0.21	0.19
0.80	-0.36	-0.10	0.07
0.90	-0.16	-0.02	0.02
1.00	0.00	0.00	0.00

The initial step involved in using Equation (1) requires that the values of U_τ and U_W be determined. A relationship between U_τ and U_W may be obtained by integrating the above equation with respect to z between the limits of z = 0 and z = δ. Using the values

$$A = \int_o^\delta \alpha \, dz = -2.2328$$

$$B = \int_o^\delta \beta \, dz = -0.4984$$

$$C = \int_o^\delta \gamma \, dz = 2.7948$$

for the integrals, the resulting expression for U_W is

$$U_W = [U(\delta_1/\delta) - 2.232 \, (U_\tau^2 - v_s U)^{1/2} - 2.794 v_s]/0.4983 \qquad (2)$$

The values of U_τ and U_W that provide the best match with the measured velocity profile and satisfy Equation (2) are considered to be the correct values.

Attempts to use this approach resulted in very poor correlation between Equation (1) and the measured profile. It was only through omission of the "law of the wake" term (U_W) that agreement between the computed and measured profiles was obtained. The dashed curves in Figure 14 represent the results of Equation (1), omitting U_W, which were interpreted to be the best fit to the measured profiles. Time did not permit the use of a curve fitting procedure to quantitatively evaluate the relative agreement between the computed and measured profiles. The corresponding values of U_τ are presented as a function of surface distance in Figure 15. Although the final values of U_τ were evaluated on a trial-and-error basis, the initial values were determined by integrating Equation (1), without the use of the U_W term, which gave the following expression for U_τ:

$$U_\tau = [v_s U + ((-U\delta_1/\delta + 2.794 v_s)/2.232)^2]^{1/2} \qquad (3)$$

With the amount of suction used on the test aircraft, the desired value of U_τ was primarily determined by the first term on the right-hand side of the above equation,

$$U_\tau \tilde{=} (v_s U)^{1/2}$$

Except for the initial profile (S_{1e} = 8.4), the agreement between the computed and measured velocity profiles is considered to be reasonable and does verify the negligible contribution of the "law of the wake" to the velocity profile obtained with relatively large amounts of suction through distinct but closely spaced suction holes.

BOUNDARY-LAYER ANALYSIS

In addition to verifying the validity of at least one of the profile shape formulations, the objectives of this study included the provision of additional information regarding the use of the boundary-layer equations for predicting the growth of the boundary layer in the test environment of high suction and adverse pressure gradient. In particular, the following discussion concerns the momentum integral equation and how well it agrees with the measured boundary-layer growth. Unfortunately, the measured data do not provide sufficient information to identify all the terms that appear in this equation. The momentum integral equation is normally used in the form

$$d\delta_2/dS + \delta_2(2 + H_{12})(1/U)(dU/dS) + v_s/U = \tau_w/\rho U^2 \qquad (4)$$

Direct measurements were made for all but the wall shear stress term (τ_w). With the measured data, therefore, it is possible to evaluate only the values of wall shear stress that are required to satisfy the integral equation, and to compare these values with any empirical formulations devised to predict this same quantity. The only relationship, known to the authors, that attempts to predict the wall shear stress for the case of suction is attributed to A. J. Sarnecki. No specific reference for this relationship can be cited. This expression is an extension of the work by Ludwieg-Tillmann (Reference 5) and is given by the equation

$$\tau_w/\rho U^2 = \theta/(R_{e\delta_2})^{0.268} \qquad (5)$$

where $\theta = 0.123 \times 10^{-0.678H_{12}} (1 + 100\, v_s/U)$

An alternate expression is considered which is based on the equation for the impervious wall shear stress by Felsch (Reference 6) with an additional term provided to allow for the functional dependency of the wall shear stress on the suction velocity. The assumed relationship is given by

$$\tau_w/\rho U^2 = (\phi + \psi)/(R_{e\delta_2})^{0.268} \qquad (6)$$

where $\phi = 0.029\,(0.93 - 1.95 \log_{10} H_{12})^{1.705}$

$\psi = f\,(v_s/U)$

Figure 16 shows the variation of the pertinent flow parameters, with surface distance, used in the momentum integral equation calculations. All data correspond to the inboard station (y = 44.5 inches) with the true velocities based on a free-stream density of 0.002098. The boundary-layer parameters correspond to the faired profiles in Figure 14. The suction velocities correspond to the data in Figure 9.

Figure 15 presents the resulting values of the friction velocity, computed with Equation (4), as a function of surface distance. The lack of agreement between the values of U_τ obtained from the Universal Profile and from the momentum integral equation for $S_{1e} > 35.0$ is a result of the apparent reduction in the boundary-layer momentum thickness measured at $S_{1e} = 47.7$. Reduced emphasis is given to the results in this region, as there were insufficient test locations in this region to properly define the local free-stream and boundary-layer characteristics. In general, the agreement between the data shown in Figure 15 is considered to be good.

Figure 17 shows the values of the sum of the functions $\phi + \psi$ (Equation 6) corresponding to the momentum integral equation calculations as a function of the suction velocity ratio. For calculation purposes, a distinct number of chordwise locations were considered in the momentum integral equation calculations. The computed values, shown as data points in Figures 17 and 18, should not be interpreted as points corresponding to the test positions. The values of θ (Equation (5)) are also shown in this figure. The use of Equation (5) would obviously result in the prediction of different boundary-layer growths than were measured in this test program.

The values of ψ required to satisfy the momentum integral equation are shown as a function of the suction velocity ratio in Figure 18. A least-squares linear curve fit to the data in Figure 18 results in

$$\psi = 7.0424 \, (v_s/U) - 0.01473 \qquad (7)$$

This curve fit was obtained neglecting the computed value corresponding to a surface distance of 46 inches ($v_s/U = 0.00557$). It should be noted that the suction velocity term in Equation (4) completely dominates the boundary-layer shape parameter terms, and the correlation of the shear stress term with the suction velocity ratio is an obvious consequence. The scatter in the computed values of data as compared to the linear curve fit would result in a significant difference in the computed boundary-layer growth based on Equation (7). This expression can only be considered as an indication of the apparent dependency of the shear stress on suction velocity. A more rigorous determination of this relationship requires more extensive testing with more sophisticated instrumentation and sufficient data points to allow more statistically significant results.

CONCLUSIONS

1. The computed suction velocities, based on the measured porosity and pressure distribution data, are considered to be representative of the actual values, although the measured blower outflow indicates that the computed suction velocities may be 10 percent high.

2. The use of the Universal Profile, proposed in Reference 4, requires that the "law of the wake" component be neglected for relatively large amounts of suction through distinct, closely-spaced suction holes.

3. The wall shear stress values required to satisfy the momentum integral equation are highly dependent upon the suction velocity (or suction velocity ratio).

Figure 1. Test Aircraft Configuration.

Figure 2. Wing Porosity Measuring Equipment.

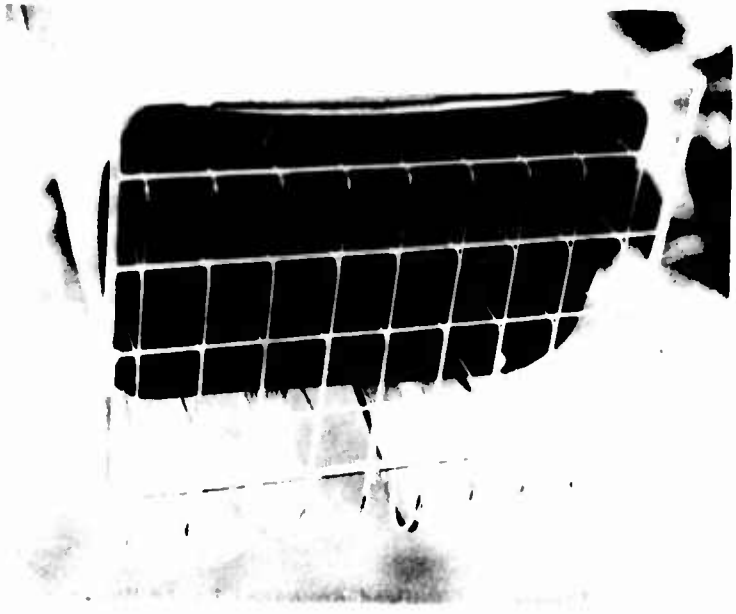

Figure 3. BLC Blower Outflow Rake.

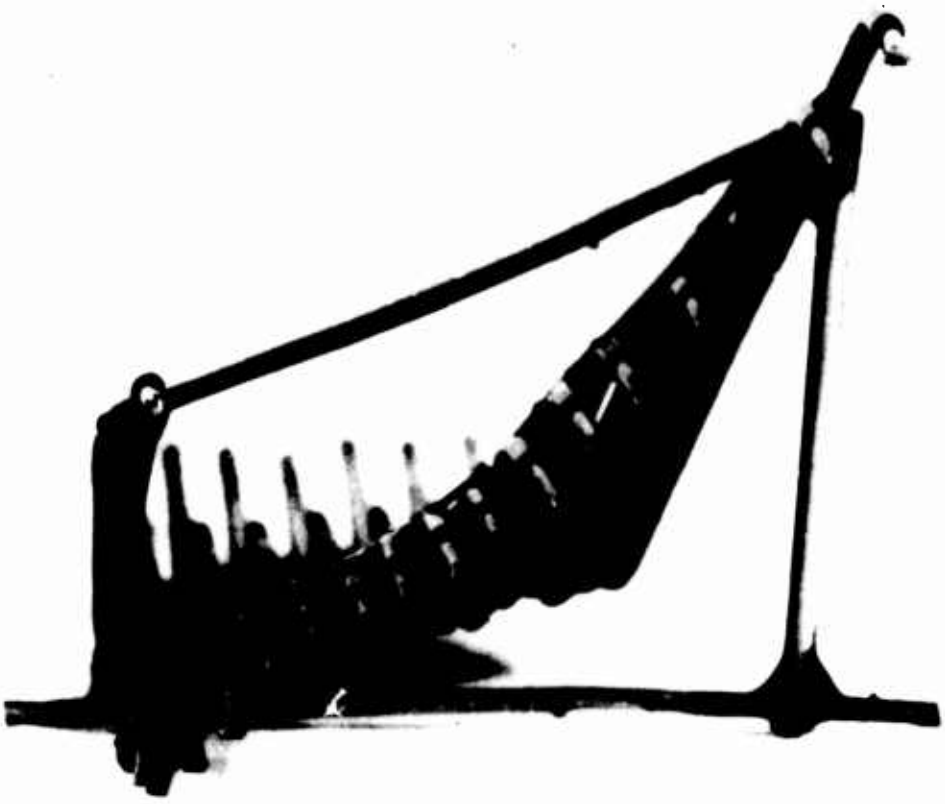

Figure 4. Curved Boundary Layer Mouse.

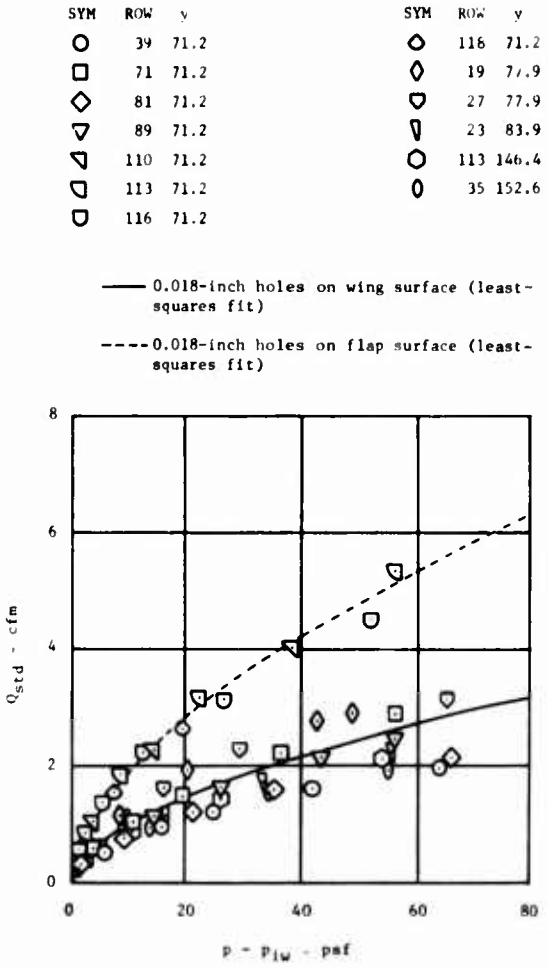

Figure 5. Porosity Data for 116, 0.018-Inch Suction Holes.

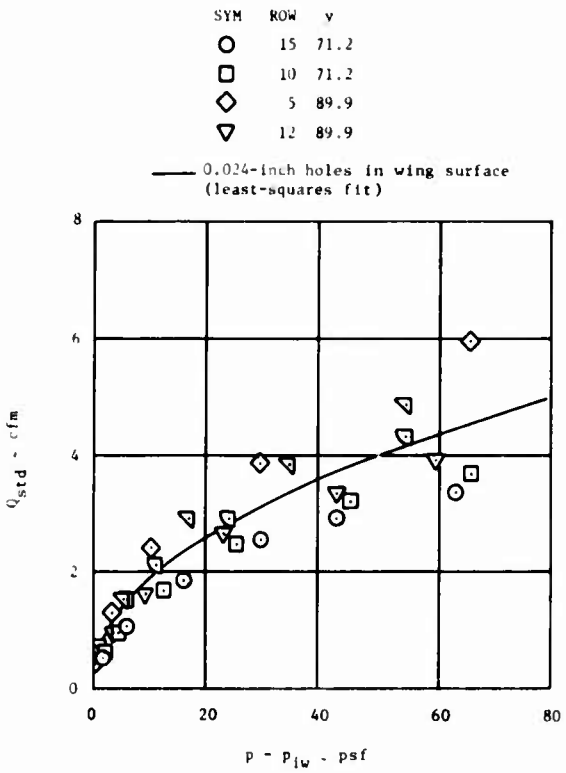

Figure 6. Porosity Data for 116, 0.024-Inch Suction Holes.

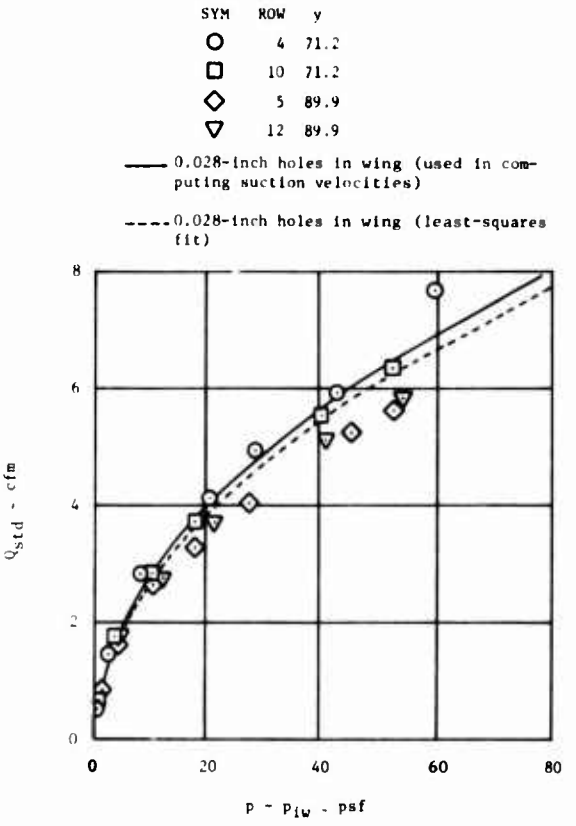

Figure 7. Porosity Data for 116, 0.028-Inch Suction Holes.

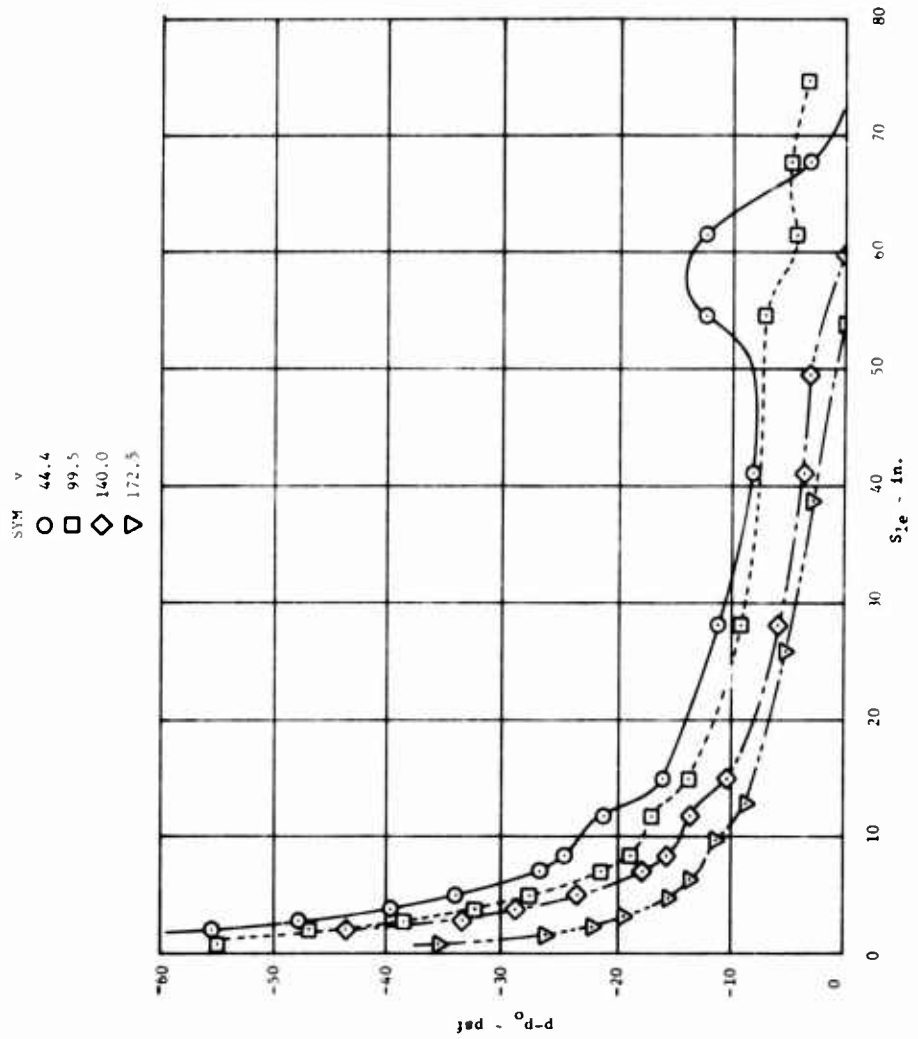

Figure 8. Pressure Distribution Data Used in Computing Suction Velocities, U_o = 36 mph.

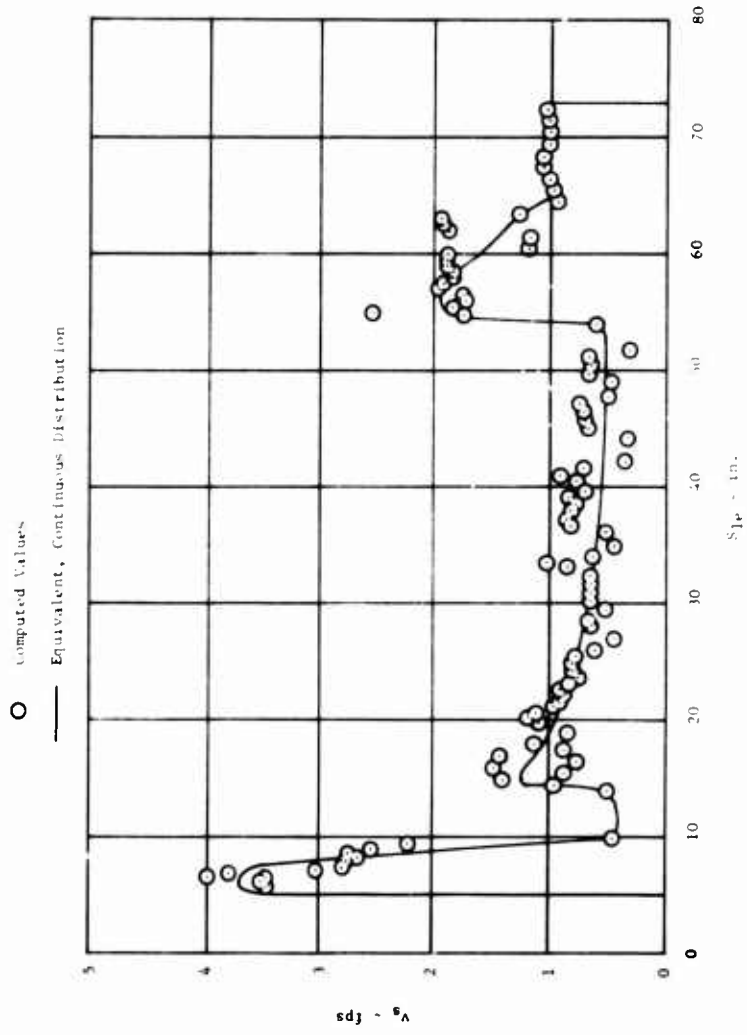

Figure 9. Suction Velocity Distribution (Equivalent Velocity), y = 44.5, U_o = 36 mph, $p_{iw} - p_o$ = -58.27 psf.

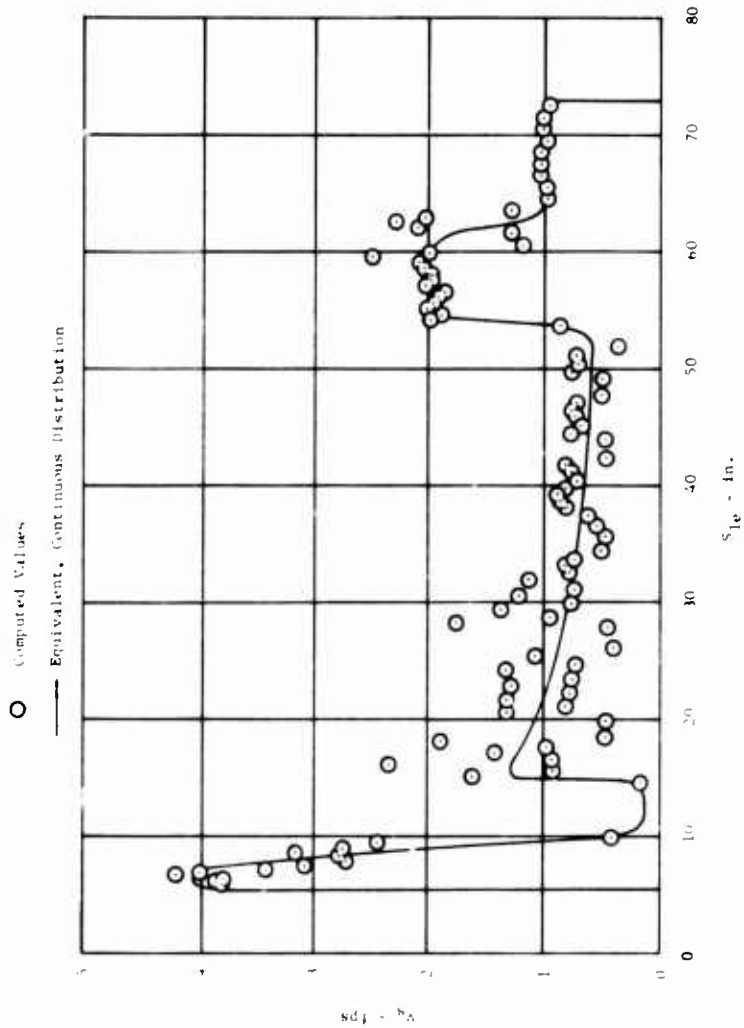

Figure 10. Suction Velocity Distribution (Equivalent Velocity), y = 99.5, U_o = 36 mph, $p_{iw} - p_o$ = -58.27 psf.

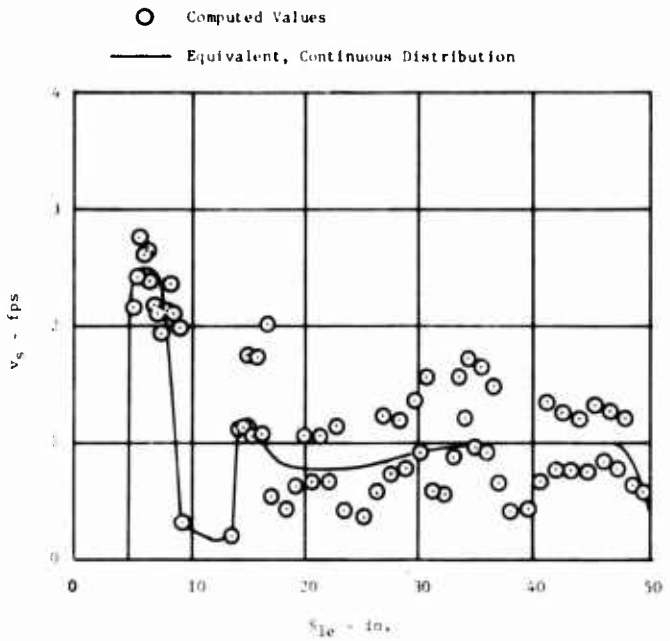

Figure 11. Suction Velocity Distribution (Equivalent Velocity), y = 140.0, U_o = 36 mph, $p_{iw} - p_o$ = -58.27 psf.

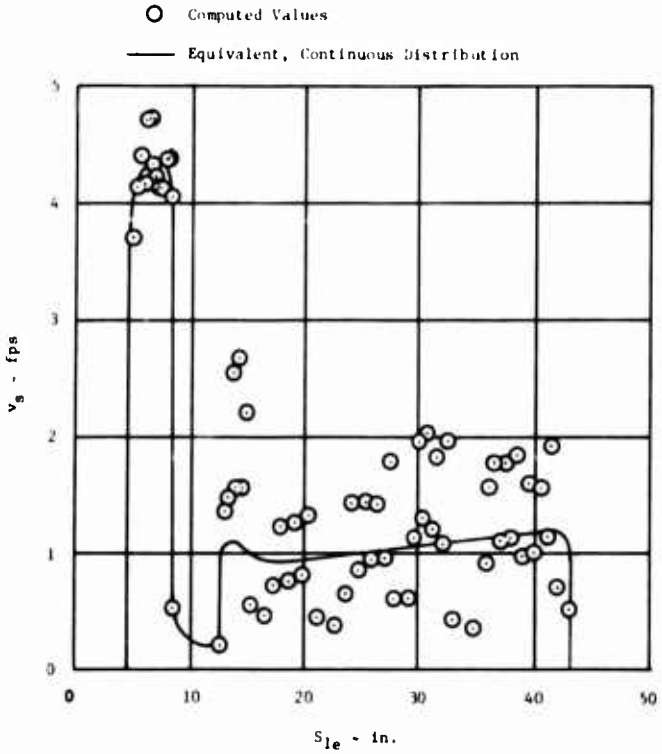

Figure 12. Suction Velocity Distribution (Equivalent Velocity), y = 172.5, U_o = 36 mph, $p_{iw} - p_o$ = -58.27 psf.

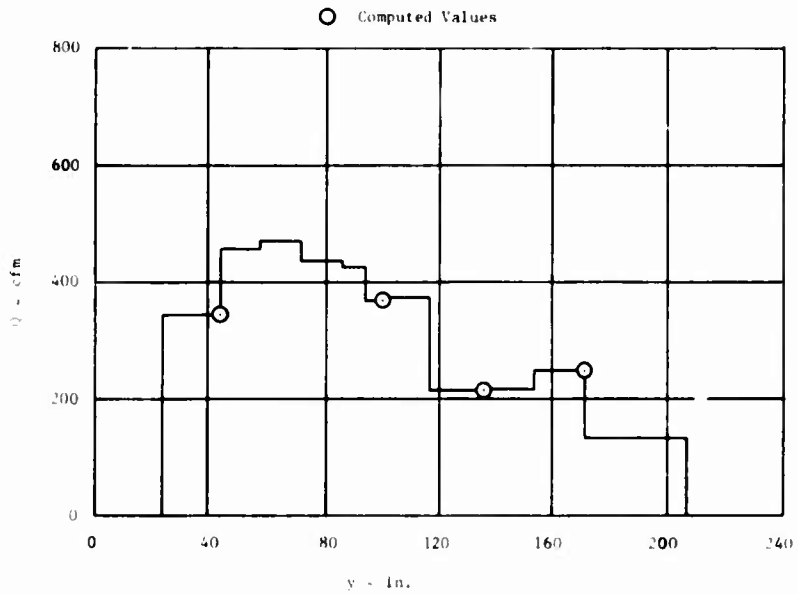

Figure 13. Spanwise, Suction Flow Distribution, U_o = 36 mph, $p_{iw} - p_o$ = -58.27 psf.

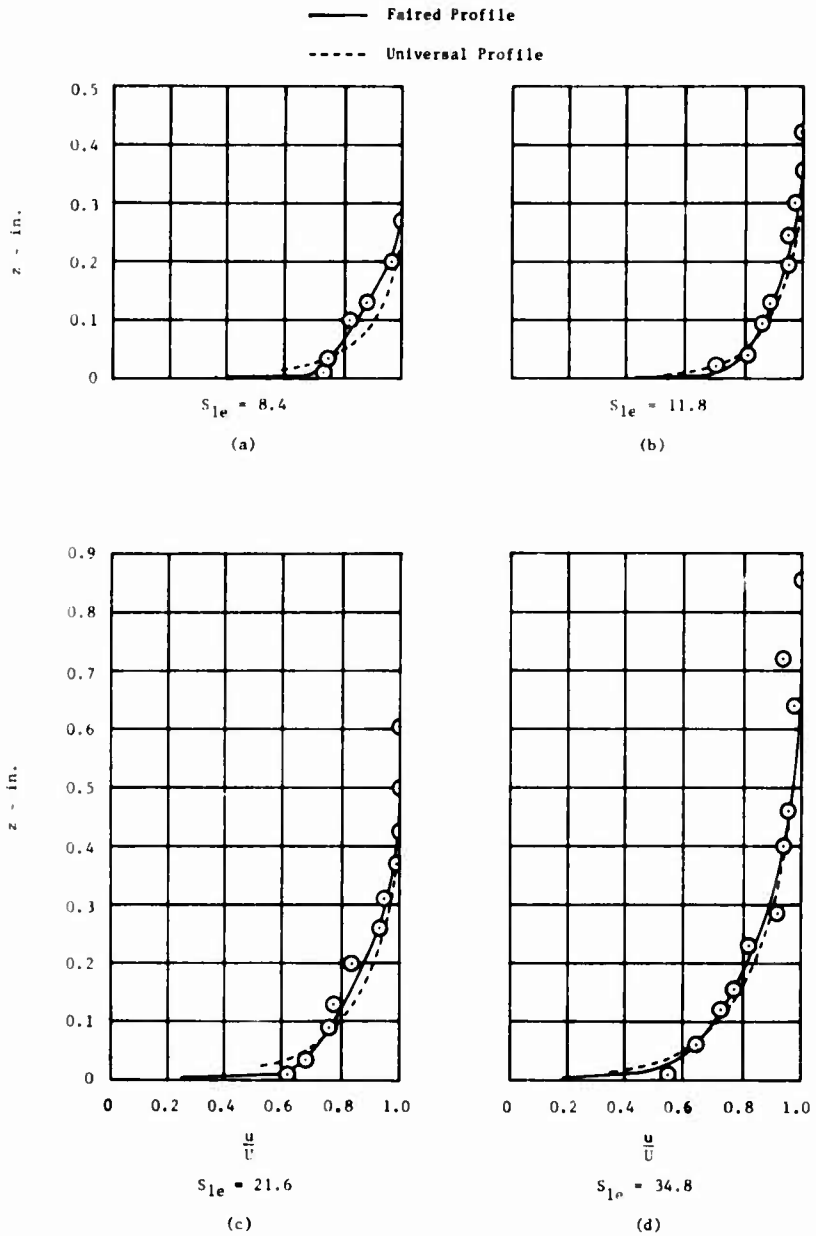

Figure 14. Boundary-Layer Velocity Ratio Profiles, y = 44.5 in., U_o = 36 mph.

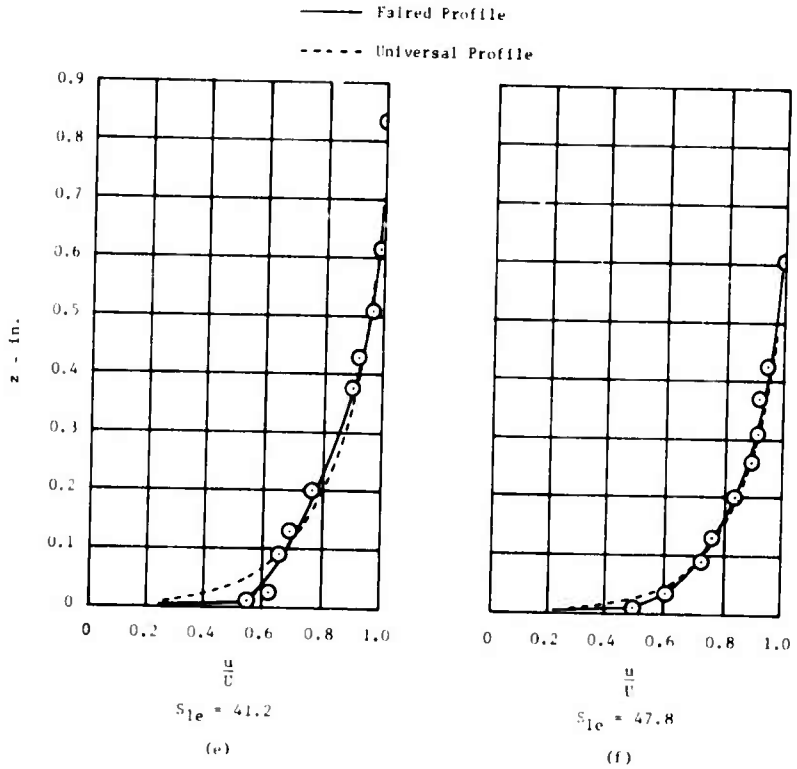

Figure 14. Concluded.

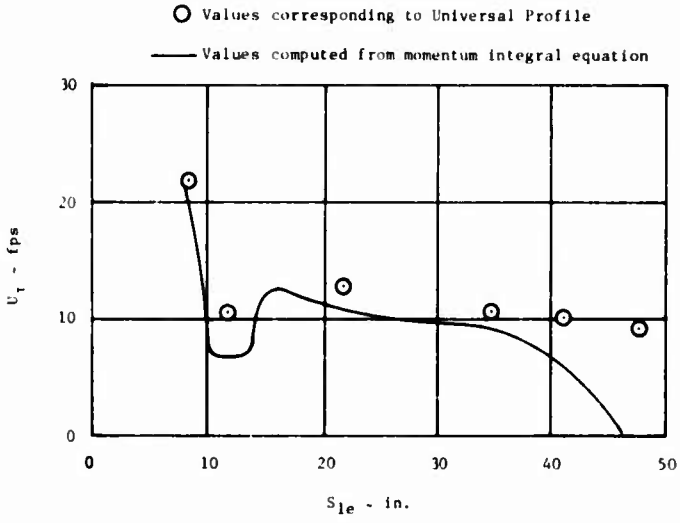

Figure 15. Friction Velocity Distribution, y = 44.5 in., U_o = 36 mph.

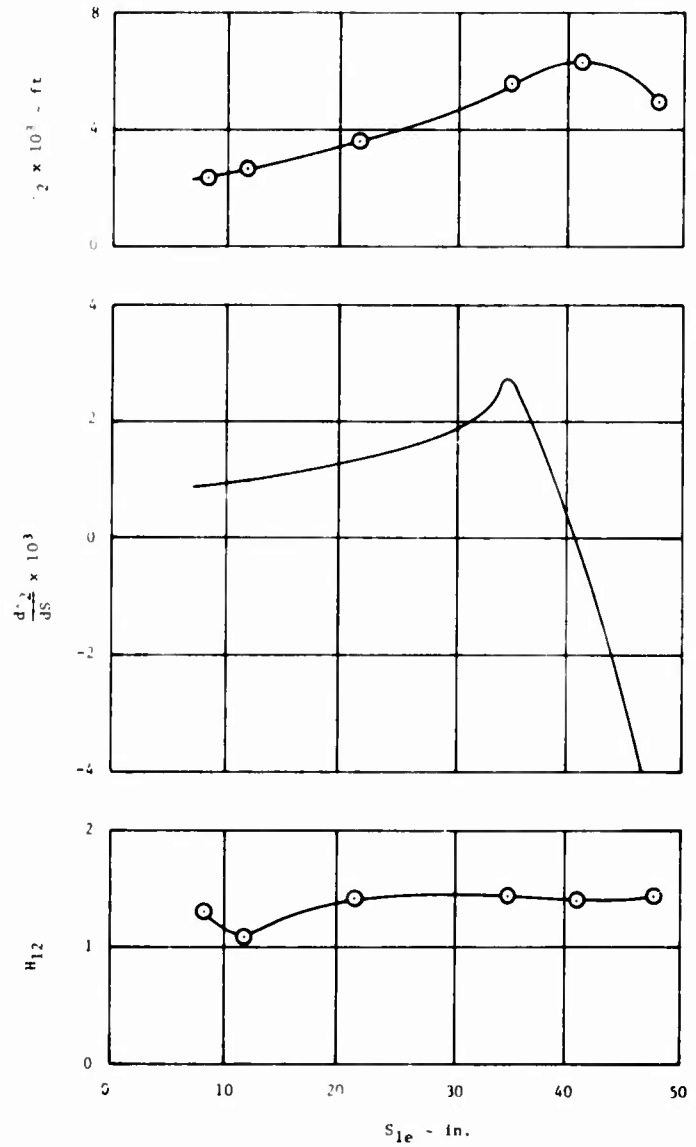

Figure 16. Boundary-Layer Characteristics Used in Analysis, y = 44.5 in., U_0 = 36 mph.

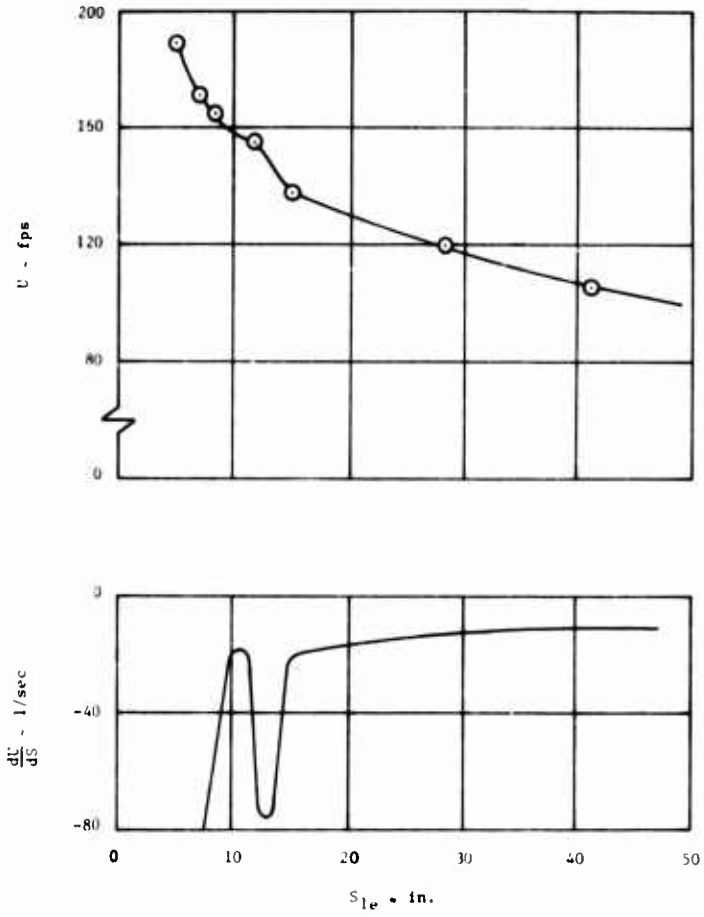

Figure 16. Continued.

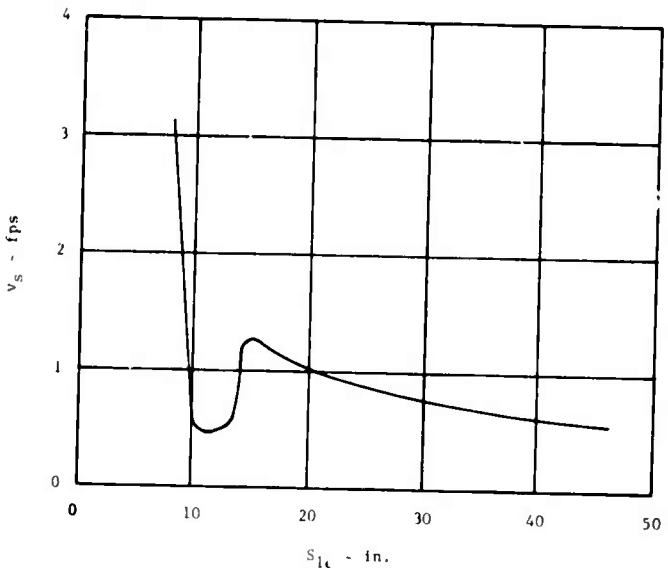

Figure 16. Concluded.

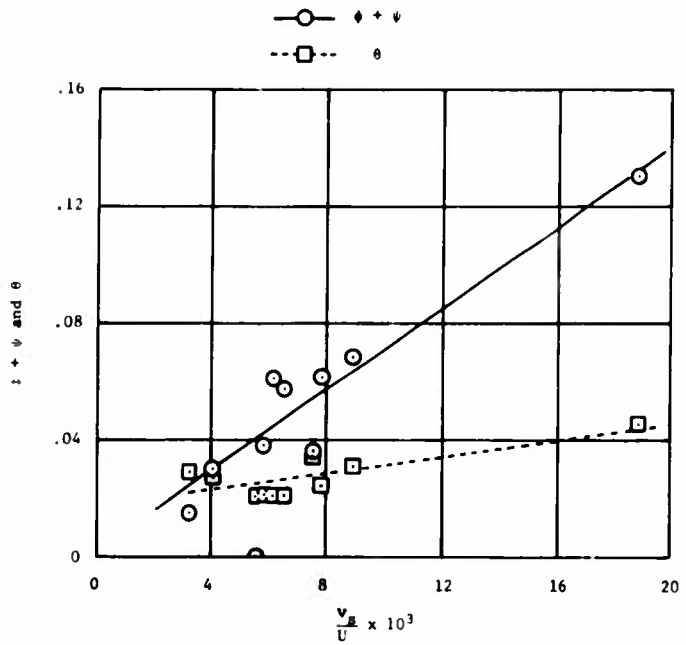

Figure 17. Shear Stress Parameters ($\phi + \psi$ and θ) Variation With Suction Velocity.

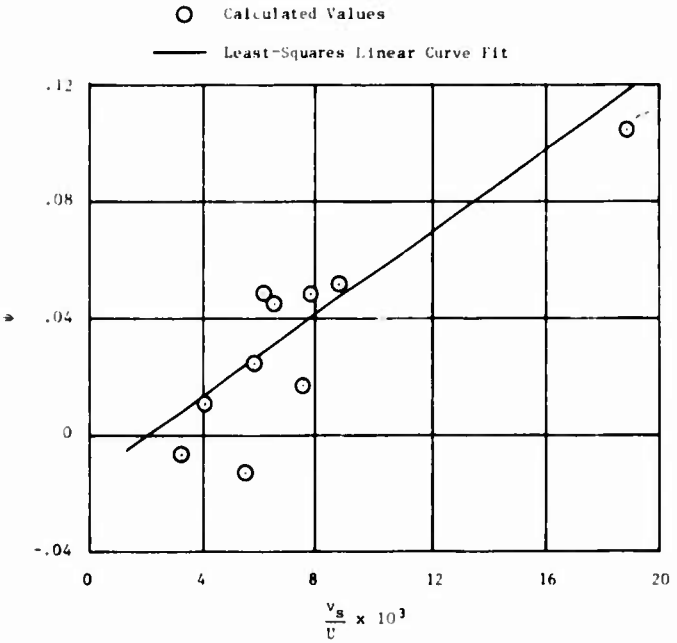

Figure 18. Shear Stress Parameter (ψ) Variation With Suction Velocity.

LITERATURE CITED

1. Roberts, S. C., Smith, M. R., and Clark, D. G., FLIGHT TEST EVALUATION OF A DISTRIBUTED SUCTION HIGH-LIFT BOUNDARY LAYER CONTROL SYSTEM ON A MODIFIED L-19 LIASON AIRCRAFT, Mississippi State University; USAAVLABS Technical Report 66-36, U. S. Army Aviation Materiel Laboratories, Fort Eustis, Virginia, June 1966, AD 635 953.

2. Coles, D. E., and Hirst, E. A. (Editors), PROCEEDINGS, COMPUTATION OF TURBULENT BOUNDARY LAYERS - 1968 AFOSR-IFP-STANFORD CONFERENCE, Volume II Compiled Data, Stanford University California, Thermosciences Division, Department of Mechanical Engineering, 1969, pp. 1-46.

3. Black, T. J., and Sarnecki, A. J., THE TURBULENT BOUNDARY LAYER WITH SUCTION OR INJECTION, Aeronautical Research Council, A. R. C. 20, 501, F. M. 2745, October 1958.

4. Cornish, J. J., A UNIVERSAL DESCRIPTION OF TURBULENT BOUNDARY LAYER PROFILES WITH OR WITHOUT TRANSPIRATION, Mississippi State University; Research Report No. 29, June 1960.

5. Ludwieg, H., and Tillman, W., INVESTIGATIONS OF THE WALL-SHEARING STRESS IN TURBULENT BOUNDARY LAYERS, NACA, TM 1285, May 1950, p. 13.

6. Kline, S. J., Markovin, M. V., Sovran, G. and Cockrell, D. J. (Editors), PROCEEDINGS, COMPUTATION OF TURBULENT BOUNDARY LAYERS - 1968 AFOSR-IFP-STANFORD CONFERENCE, Volume I Methods, Predictions, Evaluation and Flow Structure, Stanford University California, Thermosciences Division, Department of Mechanical Engineering, 1969, p. 170.